ISSN 1063-7826, Semiconductors, 2015, Vol. 49, No. 1, pp. 124–129. © Pleiades Publishing, Ltd., 2015.
Original Russian Text © Yu.G. Sadofyev, V.P. Martovitsky, M.A. Bazalevsky, A.V. Klekovkin, D.V. Averyanov, I.S. Vasil'evskii, 2015, published in Fizika i Tekhnika Poluprovodnikov, 2015, Vol. 49, No. 1, pp. 128–133.

XVIII SYMPOSIUM "NANOPHYSICS AND NANOELECTRONICS", NIZHNI NOVGOROD, MARCH 10–14, 2014

Ge/GeSn Heterostructures Grown on Si (100) by Molecular-Beam Epitaxy

Yu. G. Sadofyev[a]^, V. P. Martovitsky[a], M. A. Bazalevsky[a], A. V. Klekovkin[a], D. V. Averyanov[b], and I. S. Vasil'evskii[b]

[a] *Lebedev Physical Institute, Russian Academy of Sciences, Moscow, 119991 Russia*
^e-mail: sadofyev@hotmail.com
[b] *National Research Nuclear University MEPhI, Moscow, 115409 Russia*
Submitted May 23, 2014; accepted for publication June 15, 2014

Abstract—The growth of GeSn layers by molecular-beam epitaxy on Si (100) wafers coated with a germanium buffer layer is investigated. The properties of the fabricated structures are controlled by reflection high-energy electron diffraction, atomic-force microscopy, X-ray diffractometry, Rutherford backscattering, and Raman scattering. It is shown that GeSn layers with thicknesses up to 0.5 μm and Sn molar fractions up to 0.073 manifest no sign of plastic relaxation upon epitaxy. The lattice constant of the GeSn layers within the growth plane is precisely the same as that of Ge. The effect of rapid thermal annealing on the conversion of metastable elastically strained GeSn layers into a plastically relaxed state is examined. Ge/GeSn quantum wells with Sn molar fraction up to 0.11 are obtained.

DOI: 10.1134/S1063782615010248

1. INTRODUCTION

Alloys in the Si–Ge–Sn material system attract much interest in the context of ongoing efforts aimed at the fabrication of monolithic optoelectronic systems based entirely on Group-IVA elements. With increasing Sn content in a $Ge_{1-x}Sn_x$ alloy, the energy of the Γ7 conduction-band minimum decreases more rapidly than that of the *L*6 minimum. Simple interpolation between the band structures of germanium and gray tin (α-Sn), which is a semimetal with a band gap of –0.40 eV, predicts that an unstrained $Ge_{1-x}Sn_x$ alloy should posses a direct band gap in the range of Sn molar fractions $x \approx 0.2$–0.65, because the crossover between the indirect *L*6–Γ8 and direct Γ7–Γ8 band gaps should occur for $x \approx 0.2$ (here, Γ8 is the energy minimum of holes in the valence band at $k = 0$). The band gap E_G of the alloy in this range of compositions should vary from 0.55 eV to 0 [1]. Such a large span of the variation in E_G has not yet been confirmed experimentally due to problems with the formation of alloys with a high content of tin.

Calculations demonstrate that tensile biaxial strain in $Ge_{1-x}Sn_x$ layers, in particular, strain appearing in these layers upon heteroepitaxy, leads to the same results: both indirect and direct band gaps decrease, with the effect of strain on the direct gap being much more pronounced [2, 3]. The crossover from an indirect- to a direct-gap material may take place for a relatively small Sn molar fraction of $x = 0.02$. The available experimental data indicate that this crossover occurs for $x \geq 0.09$ [4, 5].

While the material system under discussion obviously holds much promise for both fundamental studies and applications, there are a number of factors hindering the fabrication of experimental samples with high crystalline perfection. At thermodynamic equilibrium, the solubility limit of α-Sn, which possesses a diamond-like crystal lattice and exists only at temperatures lower than 13.5°C, in germanium does not exceed 0.5%, and the solubility limit in silicon is 1.2%. The Sn atom radius (0.158 nm) is larger than that of Si and Ge (0.133 and 0.139 nm, respectively). This, along with a low value of the surface free energy of Sn, leads to a trend towards the segregation of Sn during the epitaxial growth of alloys in the Si–Ge–Sn material system. Furthermore, the lattice constant of α-Sn differs from those of Ge and Si by 14.7% and 19.7%, respectively. The lattice constant of diamond-like Si–Ge–Sn alloys follows Vegard's law. The large lattice-constant mismatch inevitably leads to problems associated with the formation of defects during the heteroepitaxy of GeSn on Si or Ge wafers.

Nevertheless, the possibility of obtaining GeSn layers with Sn molar fractions up to 0.2 in which room-temperature direct-gap photoluminescence can be observed has been demonstrated in a number of studies [6, 7]. Experimental samples of *p*–*i*–*n* diodes based on Ge/GeSn heterojunctions on a Si substrate have been fabricated. The photoresponse spectrum of these

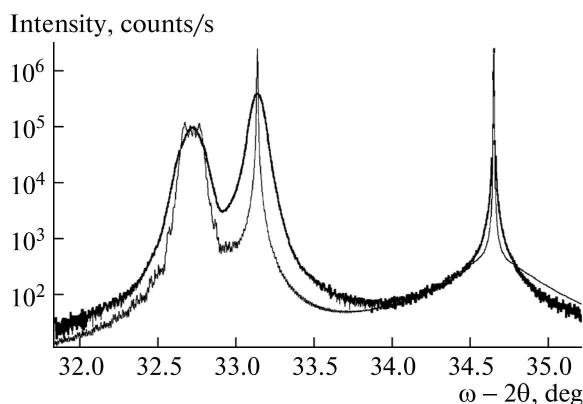

Fig. 1. Experimental and calculated rocking curves for the (004) reflection recorded for sample S041 with Ge/GeSn layers grown on Si (100). The calculated curve (thin solid line) was obtained assuming a gradient in the distribution of Sn in GeSn (left peak) from 0.036 to 0.052.

diodes covers all wavelength bands used in telecommunications applications [8, 9].

The epitaxial growth of Si–Ge–Sn structures has been conventionally performed by low-temperature (~300–400°C) low-pressure gas-phase epitaxy using silicon, germanium, and tin hydrides such as silane SiH_4, germane GeH_4 or higher germanium hydrides Ge_2H_6 and Ge_3H_8, as well as stannane SnD_4 where hydrogen is partially substituted by deuterium because of the instability of SnH_4 [10]. Molecular-beam epitaxy (MBE) has also been used for this purpose [11]. The main problem encountered in MBE is the strong tendency toward the surface segregation of tin under ultrahigh-vacuum conditions. The suppression of this effect necessitates the use of still lower growth temperatures (around 150°C). Epitaxy at such low temperatures results in a high density of intrinsic point defects, which, in particular, adversely affect the photoluminescence efficiency. MBE is the only technology available to us, and we use it to investigate the growth and properties of GeSn layers on (100)-oriented silicon wafers precoated with a buffer layer of germanium in the same MBE unit.

2. EXPERIMENTAL

The GeSn layers were grown in a Katun MBE system equipped with two electron-beam evaporators for silicon and germanium and two molecular sources of the Knudsen-cell type. These sources were used for the co-evaporation of antimony as a surfactant upon the growth of 1- to 1.5-μm-thick Ge buffer layers [12] and for the evaporation of tin upon the growth of GeSn layers. A built-in reflection high-energy electron diffractometer (RHEED) enabled in situ control of all stages of the growth process. The evaporation rates of Si and Ge were periodically measured using a quartz resonator built into the growth chamber. The properties of the grown layers were controlled by X-ray diffractometry, Rutherford backscattering (RBS), atomic-force microscopy (AFM), Auger spectroscopy, and Raman scattering.

Ge buffer layers were grown at a temperature of 650°C according to the procedure described in [12]. A two-domain reconstruction of type $(2 \times 1) + (1 \times 2)$, which is typical of the (100) orientation, was observed in the RHEED patterns for the surface of the Ge buffer layers. The half-width of the peak corresponding to the 1- to 1.5-μm-thick Ge layers in the ω–2θ rocking curves for the (004) reflection in the X-ray diffractograms was 140″–250″.

The GeSn layers were grown at a temperature of about 150°C. The Ge deposition rate was ~8 nm/min. The temperature of the Sn source was varied between 950 and 1000°C. The observed RHEED patterns indicate that, at such low growth temperatures, the epitaxy of the Ge layers proceeds with the same type of surface reconstruction as at 650°C. Meanwhile, during the growth of GeSn, fractional-order reflections disappear and shortening of the reciprocal-lattice rods takes place with the subsequent formation of V-shape reflections from facets on the surface. This pattern persists to the end of the growth process, which, in our experiments, is completed when the GeSn layer thickness reaches 0.5 μm. According to the AFM data, the rms surface roughness was about 2–3 nm, while the surface roughness of the Ge buffer layers was about 0.7 nm [12].

3. RESULTS AND DISCUSSION

X-ray diffractometry investigation of the grown structures with GeSn layers demonstrated that the Sn molar fraction can be as large as 0.073 without any sign of plastic relaxation. The lattice constant of the GeSn alloy within the growth plane was precisely the same as that of the Ge buffer layer. The lattice-constant mismatch between Ge and GeSn with a Sn molar fraction around 0.073 is about 1%. In this situation, the critical thickness for the onset of plastic relaxation, accompanied by the formation of misfit dislocations, must fall in the range of 10–100 nm, however large the spread in theoretical estimates might be [13–15]. This means that the GeSn layers grown under the conditions described above are in a metastable state. One should expect that plastic relaxation will take place upon heat treatments exceeding some critical level, which depends on the Sn molar fraction and thickness of the GeSn layers.

A typical X-ray diffractogram is shown in Fig. 1. It was obtained for sample S041, containing layers of Ge and GeSn with a Sn molar fraction of $x \approx 0.044$. The three observed peaks correspond to the GeSn and Ge epitaxial layers and the Si substrate, respectively (left to right). We believe that the noticeable broadening of the GeSn peak is caused both by the enhanced con-

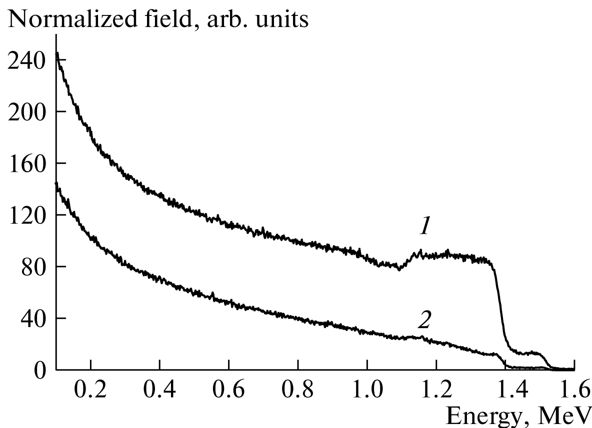

Fig. 2. Spectra of Rutherford backscattering for sample S040 with Ge/GeSn layers on a silicon wafer. The GeSn layer thickness is 0.5 μm, the Sn molar fraction is $x \approx 0.073$. The spectra are recorded (*1*) for arbitrary orientation and (*2*) under the conditions of channeling.

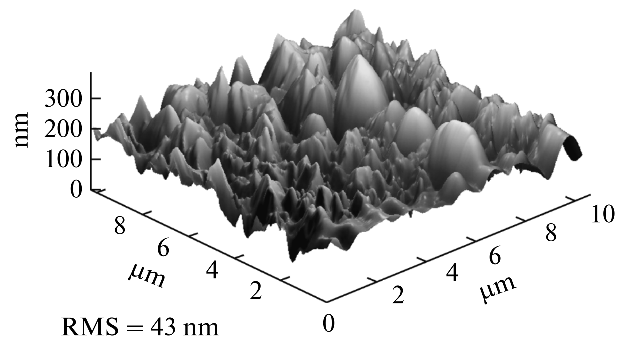

Fig. 3. AFM image of the surface profile of a GeSn layer with the Sn molar fraction $x \approx 0.044$ (sample S041) after 2-min annealing at ~350°C in the MBE growth chamber.

centration of defects and the instability of the Ge molecular-beam flux over long periods of time, required for the growth of thick layers, in the mode with stabilized power of the electron-beam evaporator. The latter mode is the only one available for the Katun MBE system. The presence of tin on the surface is detected by the appearance of a set of Auger lines typical of this element, in particular, an intense doublet at energies of 430 and 437 eV. This result should be expected, since the detectivity limit of Auger spectroscopy is $\sim 5 \times 10^{19}$ atom/cm^3 (in terms of bulk concentration). The Sn concentration in the structures under study is at a level of 10^{21} cm^{-3}.

The spectra of RBS of He ions were recorded both for structures containing only the Ge buffer layer and structures with GeSn epitaxial layers grown on a Ge buffer. These measurements were carried out in order to reveal the possible influence of the enhanced defectness of Sn-containing layers on the effect of He-ion channeling as compared to that for Ge buffer layers grown at 650°C, where the probability of the formation of intrinsic point defects is insignificant. A typical RBS spectrum, recorded for sample S040 randomly oriented with respect to the incident beam of He ions with an energy of 1.7 MeV, is shown by curve *1* in Fig. 2. Curve *2* was recorded in the mode of incident He ion channeling. The Sn molar fraction in this sample is 0.073. The energy of scattered He ions is directly proportional to the mass of atoms in the target responsible for scattering. The results for energies lower than 1.05 MeV correspond to the Ge buffer layer. The signal recorded in the energy range from 1.05 to 1.12 MeV originates from Ge atoms in the GeSn layer, and the signal in the energy range from 1.12 to 1.40 MeV originates from both Ge and Sn in the GeSn layer. At energies from 1.40 to 1.50 MeV, only scattering by Sn atoms in the GeSn layer is observed. The fraction of backscattered He ions under conditions of channeling in comparison to that under randomly orientation is 5% for samples with only a layer of Ge on Si and 10% and 13% for samples containing GeSn layers with Sn molar fractions of 0.044 and 0.073, respectively. The occurrence of channeling characterizes the crystalline perfection of the grown layers, while an increase in the backscattering rate gives evidence of the gradual degradation of the crystal alloy lattice with increasing tin content.

The Raman spectra of the layers featured three modes typical of GeSn alloys, i.e., Ge–Ge, Sn–Ge, and Sn–Sn. The positions of these modes shifted with increasing Sn molar fraction. The shift of the most intense Ge–Ge mode for the layer with a Sn molar fraction of 0.073 was ~5.5 cm^{-1}, which agrees with the available data [16].

Short-term heating of some of the samples performed in the MBE chamber immediately after growth resulted for relatively low temperatures (300–400°C) in abrupt visually observed roughening of the layer surface caused by plastic relaxation and the release of tin on the surface due to phase separation of the alloy [17]. The typical AFM image of such a surface is shown in Fig. 3. The rms roughness is about 40 nm, which is more than an order of magnitude larger than that before annealing.

In order to check the stability of the GeSn layers to heat treatments at atmospheric pressure, we carried out experiments on rapid thermal annealing of the samples in an atmosphere of high-purity nitrogen in the temperature range of 300–700°C for 2 min with subsequent control by X-ray diffractometry. It was found that the plastic relaxation of 0.5-μm-thick GeSn layers sets in at temperatures lower than those at which phase separation and accompanying surface-morphology roughening take place. The rate of the process of relaxation and tin release on the surface depends considerably on the composition of the GeSn layer. Sample S041, where the Sn molar fraction is $x \approx$ 0.044, does not lose tin upon annealing at temperatures as high as 500°C. In sample S040, where the Sn

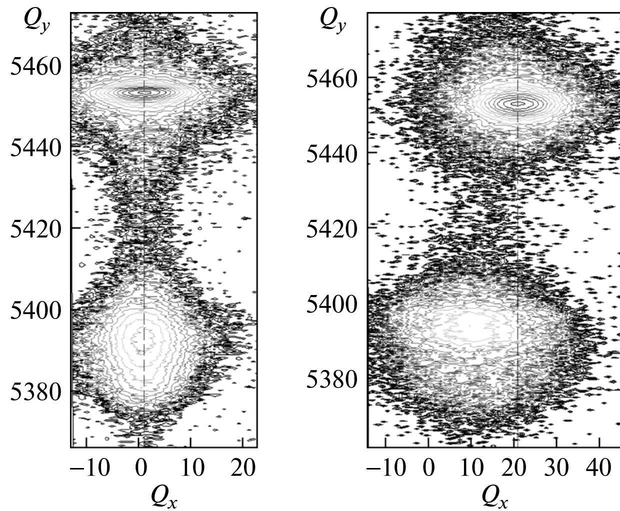

Fig. 4. Fragments of two-dimensional reciprocal-lattice patterns near the (004) node for Ge and GeSn layers (top and bottom peaks, respectively) obtained for sample S041 before and after 2-min annealing at 400°C in an inert-gas atmosphere (left and right panels, respectively).

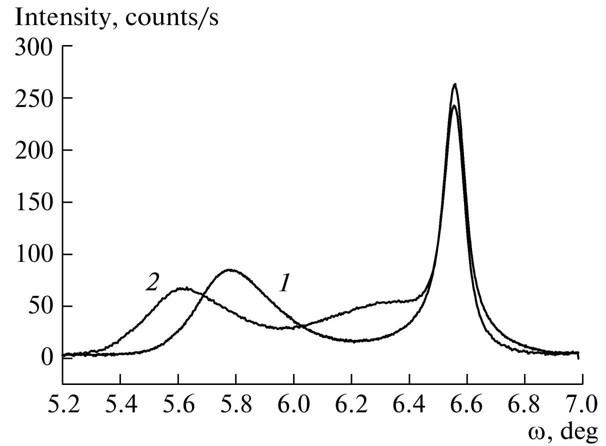

Fig. 5. Rocking curves for the (224) reflection for sample S040 with the Sn molar fraction $x \approx 0.073$ after annealing at 400°C recorded on (*1*) mirror-like and (*2*) hazy regions on the surface.

molar fraction is about 0.073, a considerable fraction of tin is released on the surface upon annealing even at 400°C.

Figure 4 shows fragments of two-dimensional reciprocal-lattice patterns near the (004) node for the Ge and GeSn layers (top and bottom peaks, respectively) in sample S041. The left and right panels show patterns obtained before and after sample annealing at 400°C, respectively. The values of Q_x and Q_y in the figure are multiplied by a factor of 1000 with respect to the actual reciprocal-lattice values. The peak shift along the vertical axis to lower values of Q_y corresponds to a larger lattice constant $a_{\perp}$ of the GeSn layer as compared to that of the Ge layer. The lack of a horizontal (Q_x-axis) shift of the GeSn peak with respect to the Ge peak in the pattern recorded immediately after growth demonstrates that the (001) crystallographic planes in the two layers are parallel, which means the absence of plastic relaxation. After annealing, the GeSn peak becomes shifted by 10 points along the Q_z axis, which corresponds to the appearance of misorientation by $\Delta\omega = 0.121°$ between the (001) planes in the Ge and GeSn layers due to plastic relaxation. A slight shift of the GeSn peak to higher values of Q_y upon annealing is accompanied by a change in the shape of this peak as a result of nonuniform plastic relaxation.

In sample S040 ($x \approx 0.073$), annealing at 400°C leads to the appearance of regions with heavy roughening of the surface profile, while most of the surface remains mirror-like. Figure 5 shows the rocking curves obtained for the (224) asymmetric reflection from the Ge and GeSn layers for the mirror-like and hazy regions (curves *1* and *2*, respectively) on the surface of sample S040. In the hazy region the GeSn peak is split in two. Figure 6 presents the rocking curves of the third analyzer crystal at the peaks of the rocking curves shown in Fig. 5. The loss of tin, leading to a shift of one of the peaks to larger diffraction angles, is accompanied, apart from a release of tin on the surface, by an increase in the tin content in the vicinity of the surface of the GeSn layer, resulting in a shift of the peak to smaller angles in comparison to the peak recorded for the mirror-like region of the sample. Thus, it can be concluded that the Sn distribution within the GeSn layer in sample S040 is inhomogeneous, and diffusion begins first of all from the layer regions with increased defect concentrations.

The dynamics of plastic relaxation and phase segregation in the GeSn epitaxial layer upon heat treat-

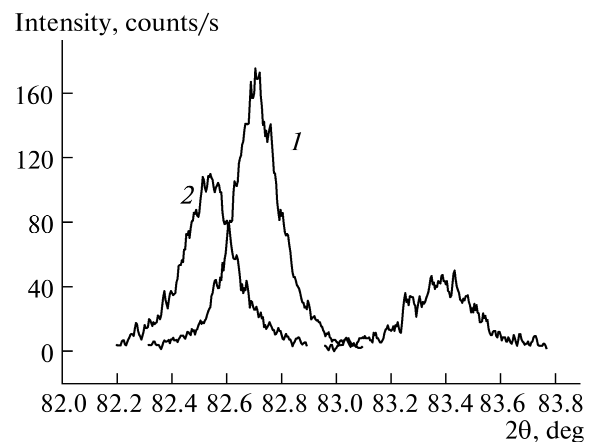

Fig. 6. Rocking curves of the third analyzer crystal at the GeSn peaks of the rocking curves shown in Fig. 5. Curves *1* and *2* correspond to mirror-like and hazy regions on the surface, respectively.

ment can be traced by monitoring the relaxed value of the lattice constant a_{relax}. For a (001)-oriented epilayer [18], $a_{relax} = \{(1 - \nu)/(1 + \nu)\}(a_\perp - a_\|) + a_\|$, where ν is the Poisson coefficient of the layer and $a_\perp$ and $a_\|$ are the lattice constants in the layer along the directions normal to the (001) plane and within that plane, respectively, which are determined from the (004) and (224) reflections, respectively. The same values were used to calculate the percentage of plastic relaxation of the GeSn layer: rel = $100 \times (a_\| - a_{Ge})/(a_{relax} - a_{Ge})$, where a_{Ge} is the lattice constant of the Ge buffer layer within the intergrowth plane (a_{Ge} = 5.6666 Å). The value of a_{Ge} is larger than a_{relax}(Ge) = 5.6577 Å. The lattice of the Ge layer, which is fully relaxed at the growth temperature, becomes tensile elastically strained at room temperature due to the larger thermal-expansion coefficient of germanium in comparison to silicon (6.1×10^{-6} and 2.33×10^{-6} cm K^{-1}, respectively).

The lattice constant of the GeSn layer in sample S041 (Sn molar fraction $x \approx 0.044$) measured immediately after growth was 5.6939 Å. It did not change upon annealing at 400°C (a_{relax} = 5.6939 Å, (400) reflection) and even slightly increases upon annealing at 500°C (a_{relax} = 5.7017 Å, (500) reflection), while the degree of plastic relaxation increases from 47.6% after annealing at 400°C to 67.2% after annealing at 500°C. Sample S040 demonstrates quite different behavior. Due to a higher tin content (a_{relax} = 5.7188 Å, $x \approx 0.073$), even annealing at 300°C causes a reduction in the tin content (a_{relax} = 5.7052 Å, (300) reflection). At 400°C, the partial disproportionation of the GeSn-layer composition into two different tin concentrations is observed; after annealing at 500°C, a major fraction of tin is released on the surface of the epitaxial layer.

We also fabricated Ge/GeSn/Ge quantum wells with a thickness of 7 nm and a tin content of 0.11. The annealing of a quantum-well sample at temperatures up to 600°C does not lead to noticeable modifications of the X-ray diffractogram, because heteroepitaxial strain accumulated in the thin quantum-well layer does not attain the high levels typical of 0.5-μm-thick GeSn layers considered above.

4. CONCLUSIONS

Thus, we have demonstrated that GeSn layers of above-critical thickness grown on relaxed Ge buffer layers by MBE at low temperatures (~150°C) do not exhibit signs of plastic relaxation. For structures with Sn molar fractions up to $x \approx 0.07$, the lattice constant of the GeSn layer within the intergrowth plane exactly coincides with that of the Ge buffer layer on the Si substrate; i.e., the GeSn layer experiences compressive biaxial strain. In turn, the Ge layer, which is fully plastically relaxed at the growth temperature, experiences tensile biaxial strain at room temperature due to the difference in the thermal expansion coefficients of silicon and germanium.

The state of the strained GeSn layer is metastable. Plastic relaxation occurs upon heat treatments at moderate temperatures (400–600°C, depending on the tin content in the layer). The relaxation is accompanied by the partial phase separation of GeSn: first, there is an increase in the average tin content in more stable fragments of the layer, and then the release of tin at the surface of the epilayer takes place. The incorporation of tin into the underlying Ge buffer layer can also occur. This imposes significant restrictions on the allowable range of heat treatments that can be applied during the fabrication of devices based on GeSn structures. Meanwhile, higher temperatures can be used for Ge/GeSn/Ge quantum-well structures due to lower level of accumulated heteroepitaxial strain. The largest molar fraction of Sn in the grown GeSn layers is $x \approx 0.11$.

The formation of a metastable elastically strained state of $Ge_{1-x}Sn_x$ layers of above-critical thickness upon their growth by MBE at low temperatures on Si wafers coated with Ge prevents their use as stressors for the subsequent deposition of $Ge_{1-y}Sn_y$ layers with $y < x$. A stressor layer serves to form tensile biaxial strain in the working $Ge_{1-y}Sn_y$ layer in order to attain direct-gap band structure at relatively low Sn molar fractions. To obtain plastically relaxed $Ge_{1-x}Sn_x$ layers by MBE, it is reasonable to grow them directly on Si without using intermediate Ge buffer layers. In this case, the lattice-constant mismatch between the materials forming a Si/GeSn heterojunction will be close to 5% instead of ~1% for Ge/GeSn, which will inevitably result in plastic relaxation of the epitaxial layer for relatively small thicknesses (about 100 nm).

ACKNOWLEDGMENTS

This study was supported by the Russian Foundation for Basic Research (project no. 13-02-00680) and the Russian Science Foundation (project no. 14-22-00273).

REFERENCES

1. S. Ogus, W. Paul, T. F. Deutsch, B. Y. Tsaur, and D. V. Murphy, Appl. Phys. Lett. **43**, 848 (1983).
2. R. A. Sofer and L. Friedman, Superlat. Microstruct. **14**, 189 (1993).
3. O. Gurdal, P. Desjardins, J. R. A. Carlsson, N. Taylor, H. H. Radamson, J.-E. Sundgren, and J. E. Greene, J. Appl. Phys. **83**, 162 (1998).
4. G. He and H. A. Atwater, Phys. Rev. Lett. **79**, 1937 (1997).

5. J. Mathews, R. T. Beeler, J. Tolle, C. Xu, R. Roucka, and J. Kouvetakis, J. Menéndez, Appl. Phys. Lett. **97**, 221912 (2010).

6. R. Ragan and H. A. Atwater, Appl. Phys. Lett. **77**, 3418 (2000).

7. G. Grzybowski, R. T. Beeler, L. Jiang, D. J. Smith, J. Kouvetakis, and J. Menendez, Appl. Phys. Lett. **101**, 072105 (2012).

8. J. Mathews, R. Roucka, J. Xie, S.-Q. Yu, J. Menéndez, and J. Kouvetakis, Appl. Phys. Lett. **95**, 133506 (2009).

9. S. Su, B. Cheng, C. Xue, W. Wang, Q. Cao, H. Xue, W. Hu, G. Zhang, Y. Zuo, and Q. Wang, Opt. Express **19**, 6400 (2011).

10. M. R. Bauer, C. S. Cook, P. Aella, J. Tolle, J. Kouvetakis, P. A. Crozier, A. V. G. Chizmeshya, D. J. Smith, and S. Zollner, Appl. Phys. Lett. **83**, 3489 (2003).

11. H. Lin, R. Chen, W. Lu, Y. Huo, T. I. Kamins, and J. S. Harris, Appl. Phys. Lett. **100**, 102109 (2012).

12. Yu. G. Sadofyev, V. P. Martovitskii, and M. A. Bazalevskii, Bull. Russ. Acad. Sci.: Phys. **78**, 29 (2014).

13. J. W. Mattehews and A. E. Blakeslee, J. Cryst. Growth **27**, 118 (1974).

14. R. People and J. Bean, Appl. Phys. Lett. **47**, 322 (1985).

15. F. Y. Huang, Phys. Rev. Lett. **85**, 787 (2000).

16. H. Lin, R. Chen, Y. Huo, T. I. Kamins, and J. S. Harris, Appl. Phys. Lett. **98**, 261917 (2011).

17. V. G. Deibuk and Yu. G. Korolyuk, Semiconductors **36**, 1073 (2002).

18. A. Krost, G. Bauer, and J. Woitok, in *High Resolution X-ray Diffraction in Optical Characterization of Epitaxial Semiconductor Layers*, Ed. by G. Bauer and W. Richter (Springer, 1996), p. 287.

Translated by M. Skorikov